ISSN 1330-3651 (Print), ISSN 1848-6339 (Online)
Received: 11 February 2025; Accepted: 20 November 2025

https://doi.org/10.17559/TV-20250211002360
Original scientific paper

Investigating the Influence of Cutting Insert Angles on Dimensional Deviation and Surface Roughness During Turning of Ti6Al4V Alloy

Djordje VUKELIC, Aleksandar MILOSEVIC, Goran SIMUNOVIC, Vitalii IVANOV, Zeljko SANTOSI, Mario SOKAC, Slobodan MITROVIC

Abstract: In the study, the influence of rake angle, clearance angle, inclination angle, approach angle and nose angle on the dimensional deviation and roughness of the machined surface during dry turning of Ti6Al4V alloys was investigated. The experimental investigation utilized a custom design of experiments. The results indicated that the dimensional deviation varied between 0.053 mm and 0.081 mm, while the surface roughness ranged from 1.892 mm to 2.141 mm, depending on the different combinations of insert angles. An analysis of the results showed significant effects of both the main and quadratic interactions of the input parameters on the output parameters. Notably, altering the angles of the cutting insert affected dimensional deviation by 52.83% and surface roughness by 13.16%. Additionally, a strong correlation was found between the output parameters. Confirmation experiments were conducted to validate the developed predictive equations, and the percentage errors demonstrated the accuracy of the modelling process.

Keywords: approach angle; clearance angle; dimensional deviation; inclination angle; nose angle; rake angle; surface roughness; turning

1 INTRODUCTION

Titanium alloys are known for their higher corrosion resistance, lower density, high specific strength, and low modulus of elasticity. These properties make them valuable in various industries, including aerospace, automotive, marine, and medical applications. There are many types of titanium alloys, with Ti6Al4V being one of the most widely used. Ti6Al4V possesses characteristics such as low thermal conductivity, high hardness, high chemical reactivity, and high specific strength, placing it in a category of materials that are difficult to cut. Machining this alloy generates high forces, elevated temperatures, and high contact pressures, which can lead to significant wear on cutting inserts. Additionally, these conditions may result in vibrations and work hardening, adversely affecting dimensional accuracy and surface finish. Therefore, it is crucial to carefully select all input parameters during the machining process to ensure optimal performance.

In the past, the turning of Ti6Al4V alloy has been studied from various aspects. Che-Haron and Jawaid [1] investigated surface roughness, hardness and hardening. The machined surface experienced a change in microstructure and an increase in hardness. Strong plastic flow was observed in a worn tool. Ramesh et al. [2] investigated the influence of cutting parameters on surface roughness using the Taguchi method. The surface roughness increased with increasing feed and decreased with increasing cutting speed and depth of cut. Jianxin et al. [3] investigated the diffusion of elements from the workpiece to the cutting tools and vice versa. The diffusion of elements from the titanium alloy into the carbide tool through the tool-chip interface led to a change in the composition of the tool substrate and accelerated tool wear. Tsourveloudis [4] used response surface methodology (RSM) and fuzzy logic to predict surface roughness. The feed had the greatest influence on the surface roughness. Fan et al. [5] investigated the influence of coated and uncoated carbide tools on cutting forces. The results showed that different coating types generate different components of the radial cutting forces. Wang et al. [6] studied the influence of turning parameters on tool life. Higher tool life values are achieved at lower cutting speeds and greater depth of cut. Xie et al. [7] proposed various uncoated micro grooved tools on the rake faces. The microgrooves on the rake face help to reduce the friction of cutting chip frictions and eliminate the cutting heat. Kosaraju and Anne [8] investigated the effects of turning parameters on cutting force and surface roughness using RSM. The cutting force increased with increasing depth of cut and feed and decreased with increasing cutting speed and rake angle, while the surface roughness decreased with increasing cutting speed and rake angle and increased with increasing depth of cut and feed. Sun et al. [9] investigated changes in tool geometry and presented the correlation of cutting forces with the evolution of tool wear. The results showed that there is a direct correlation between cutting speed, tool wear and cutting forces. Sun et al. [10] investigated the effects of turning conditions on tool life. The main failure mechanisms of the cutting tool were chipping, notching, adhesion and cratering. The main failure mechanisms were adhesion, craters and diffusion. Chetan et al. [11] discussed the wear characteristics of TiN-coated cemented carbide inserts. Micro-chipping, micro-fracture, built-up edge and abrasion were the main wear mechanisms. Sargade et al. [12] presented the effects of turning parameters on surface roughness and cutting force. By increasing the cutting speed and reducing the feed, a better surface roughness and a lower cutting force were achieved. Umbrello et al. [13] proposed a finite element model to simulate the microstructure, plastic deformation and hardness variations. The cutting speed had the greatest influence. Celik et al. [14] investigated the effects of cutting parameters and tool coating method on tool wear and surface roughness. Tool wear increased with increasing cutting speed, feed and depth of cut. The surface roughness deteriorated with increasing feed and depth of cut. Sanchez Hernandez et al. [15] analysed the influence of cutting speed and feed on chip morphology and geometry. As the feed increases, the height of the valleys, the height of the peaks, the equivalent chip thickness and the transverse section area increase. Caggiano [16] implemented a machine learning method based on the acquisition and machining of cutting force, acoustic emission and vibration sensor signals to monitor cutting

tool flank wear. An accurate diagnosis of flank wear was achieved using artificial neural networks (ANN) with the features of principal component analysis. Dargusch et al. [17] explored the chip microstructure and deformation mechanisms. The extent of tool wear had a significant influence on the degree of chip segmentation and the predominant types and amounts of deformation. Sanchez Hernandez et al. [18] analysed the influence of cutting speed and feed on tool wear and cutting force. The cutting force showed a general trend towards an increase with both turning parameters. The cutting speed showed a slightly higher influence on crater wear and the feed showed a higher influence on flank wear. You et al. [19] used the Taguchi method to investigate the influence of tool material, cutting speed and feed on flank wear, surface roughness and cutting force. The carbide tool showed the best tool life. The greatest tool wear was due to adhesion. The feed had the greatest influence on surface roughness. Liang et al. [20] investigated the surface quality after dry turning. The results show that there is a direct correlation between tool wear and surface integrity. Wang et al. [21] investigated the influence of electromagnetic coupling machining on cutting temperatures and flank wear. The results show that the treated cutting tool generates lower cutting temperatures and less tool wear. Kumar and Misra [22] modelled the tool wear as a function of turning parameters using the RSM method and ANN. Tool wear increased with an increase in cutting speed. De Maddis et al. [23] evaluated the influence of cutting speed and feed on cutting temperature and surface roughness. Cutting speed and feed primarily affected the surface roughness. The cutting speed also significantly influenced the temperature. Guvenc et al. [24] implemented active vibration control based on sliding mode control to reduce and eliminate vibration. The surface roughness decreased significantly after the application of active vibration control. Martin-Bejar [25] analysed the influence of cutting speed and feed on roughness, geometry deviations and hardness. The feed had the greatest influence on the geometry deviations, while the cutting speed mainly influenced the hardness. Cozzolino et al. [26] investigated the surface roughness, specific cutting energy and energy consumption during turning of titanium workpieces produced by electron beam melting. The results showed that dry turning can lead to lower energy consumption. Feed and depth of cut can be varied by fixing the cutting speed without significantly affecting the surface roughness.

The turning of Ti6Al4V alloys has been explored from various perspectives, with most investigations being experimental in nature. One major drawback of experimental research is that it can be both costly and time-consuming. However, utilizing modelling techniques can significantly reduce both time and expenses [27]. A variety of modelling approaches have been employed to analyse the turning process, including regression models [28, 29], artificial neural networks [30], and fuzzy modelling [31]. These models have assessed the influence of factors such as feed, depth, cutting speed, and tool material on output parameters, which include tool life, wear mechanism, cutting force, cutting temperature, hardness, and energy consumption. Among these parameters, surface roughness has been studied most frequently [32]; conversely, dimensional accuracy, despite being a critical output parameter, has received relatively little research attention [33, 34, 35]. Overall, there is currently no universal model that adequately defines the relationship between input and output parameters in the turning process, rendering it inapplicable in all scenarios. Additionally, no research has comprehensively examined the impact of insert angles on both dimensional accuracy and surface roughness in the turning of Ti6Al4V alloys.

This study aims to analyse and model the influence of five angles of cutting inserts on the dimensional deviation and surface roughness during the dry turning of Ti6Al4V alloy, contrasting with previous research. The input parameters - rake angle, clearance angle, inclination angle, approach angle, and nose angle - were evaluated for their effects on the output parameters, which are surface roughness and dimensional deviation. Regression equations were formulated to establish a functional relationship between the cutting insert angles and the resulting dimensional deviation and surface roughness. Additionally, a correlation between the output parameters, specifically between surface roughness and dimensional deviation, was identified.

2 METHODOLOGY

The research methodology is illustrated in Fig. 1. The experiments were conducted using workpieces with dimensions of Ø 45 × 425 mm, made from Ti6Al4V alloy.

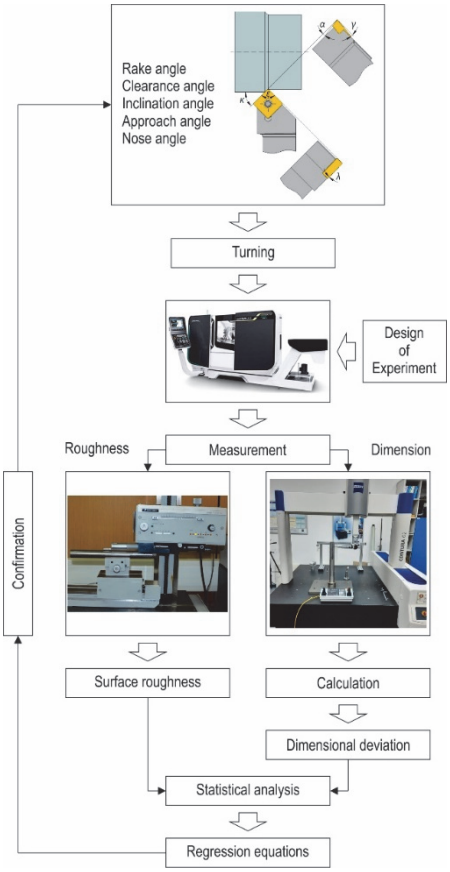

Figure 1 Research methodology

The longitudinal external turning was conducted using a GildemeisterCTX 310 CNC lathe. Each experiment employed a new cutting insert, which had the following

common characteristics: a thickness of 4.8 mm, substrate material of HC, and a coating comprising CVD TiCN + Al_2O_3 + TiN with a thickness of 10 μm. The nose radius was 0.8 mm.

Following the recommendations of the cutting insert manufacturer, the turning parameters were set as follows: cutting speed (v_c) of 40 m/min, feed (f) of 0.1 mm/rev, and depth of cut (a_p) of 1 mm.

The input parameters for the experiment included various cutting insert angles: rake angle (γ), clearance angle (α), inclination angle (λ), approach angle (κ) and nose angle (ε). The specific levels of these input parameters are detailed in Tab. 1. Theoretically, cutting insert angles could be treated as continuous variables; however, in reality, they have discrete values, as manufacturers of cutting inserts produce them with precisely defined and common values. Some of the values of the angles of cutting inserts are defined by standards (ISO 1832), while others are common among all manufacturers of cutting inserts. The rake angle is defined by the manufacturer as a common value for the positive turning insert style. Clearance angle is defined by the standard. Three standard clearance angles were selected. Inclination angle is varied with the change of insert shims. Standard shims are used to vary this inclination angle. Approach angle is defined by the cutting insert holder. The combination of the insert shape and toolholder defines this angle. Nose angle is defined by the standard, i.e. standard shape of the cutting insert. The following shapes correspond to the selected corners: rhombic insert shape, triangular insert shape and square insert shape. Input parameter levels (cutting insert angles) selected according to possible combinations offered by manufacturers. Cutting inserts used in the research can be purchased from the manufacturer for use in real production systems.

Table 1 Input parameter levels

Input parameters	Minimum level	Medium level	Maximum level
γ / °	6	8	10
α / °	5	7	11
λ / °	0	1	2
κ / °	60	75	90
ε / °	35	60	90

The output parameters analysed were dimensional deviation (Δd) and surface roughness (R_a).

Before and after turning, the dimension (diameter) was measured, and the Δd was calculated. Δd represents the deviation of the obtained measure from the required measure, i.e.:

$$\Delta d = d_{2n} - d_{2m} = \left(d_{1m} - 2 \cdot a_p\right) - d_{2m} \quad (1)$$

where: d_{2n} is the required diameter value after turning, and d_{2m} is the measured diameter value after turning, d_{1m} is the measured diameter value before turning and a_p is the depth of cut.

Diameter measurement was performed on a Zeiss Contura G2 coordinate measuring machine using the point-by-point method.

Additionally, R_a was measured after processing using a Talisurf measuring device. This measurement used a Gaussian filter with a sampling length of 0.8 mm and an evaluation length of 4 mm.

The experiment plan and process modelling were developed based on a customized experiment design. A statistical power analysis indicated that 48 experimental points provided a sufficient level of confidence to identify real effects. The experimental research was conducted using a randomized design to minimize systematic errors and unwanted external factors.

Following the experimental results, statistical analysis, process modelling, and the generation of regression equations were performed. A correlation analysis was subsequently conducted to examine the relationship between R_a and Δd, quantifying the interrelationship of these output parameters. The accuracy and reliability of the regression models were confirmed through additional confirmation experiments.

3 RESULTS

The results of measurements and calculations are presented in Tab. 2. Measurements were conducted three times, and the table displays the mean values of R_a and Δd for various combinations of cutting insert angles. The variability of the measured results is assessed absolutely using the standard deviation (σ) and relatively using the coefficient of variation (CV).

The measured values - ranging from 1.909 μm to 2.141 μm for R_a and from 0.055 mm to 0.081 mm for Δd - demonstrate the ability to control the output parameters and highlight their dependence on the combination of input parameters.

The calculated standard deviations, which for R_a range from 0.004 μm to 0.020 μm and for Δd from 0.001 mm to 0.003 mm, show that the measured values are close to the mean, with no significant deviations. This small variability indicates that the measurement results are reliable.

The calculated coefficients of variation - ranging from 0.207% to 1.033% for R_a and from 1.351% to 4.000% for Δd - demonstrate that the standard deviation is small relative to the mean values. As a result, the relative variability is low, and the calculated mean values can be considered reliable.

3.1 Statistical Analysis

Statistical analysis of the measured results for R_a and Δd was performed in JMP software using A-optimal criterion in order to determine the most important factors and their effects on the output parameters. The statistical analysis is based on a model with main effects, their quadratic effects and two-factor interactions, which provides a detailed understanding of the complex relationships between input and output parameters.

Statistically significant effects in the model were identified using the effect summary shown in Tab. 3. Effects with a p-value of less than 0.05 are statistically significant, meaning that their presence in the model has a significant impact on R_a and Δd. The effects are ordered by Log Worth values, which are defined as -log10 (P-value). Effects with higher Log Worth values have greater statistical significance in the model.

Table 2 Results

No.	γ / °	α / °	λ / °	κ / °	ε / °	R_a / µm	σ_{R_a} / µm	CV_{R_a} %	Δd / mm	$\sigma_{\Delta d}$ / mm	$CV_{\Delta d}$ / %
1	10	7	4	75	90	2.000	0.018	0.900	0.062	0.002	3.226
2	6	11	2	90	35	2.077	0.016	0.770	0.075	0.003	4.000
3	10	5	2	90	90	2.027	0.018	0.888	0.068	0.001	1.471
4	6	11	4	90	90	2.040	0.018	0.882	0.071	0.002	2.817
5	10	5	4	75	90	2.018	0.014	0.694	0.066	0.001	1.515
6	10	7	0	60	90	1.956	0.014	0.716	0.059	0.001	1.695
7	10	5	2	60	60	2.003	0.014	0.699	0.065	0.002	3.077
8	10	5	0	75	35	2.046	0.018	0.880	0.069	0.002	2.899
9	10	11	2	60	35	2.078	0.014	0.674	0.076	0.003	3.947
10	10	11	4	60	60	2.060	0.012	0.583	0.074	0.001	1.351
11	6	11	4	75	35	2.069	0.008	0.387	0.074	0.002	2.703
12	10	11	0	75	90	2.025	0.006	0.296	0.072	0.002	2.778
13	6	7	4	60	35	2.000	0.012	0.600	0.061	0.002	3.279
14	8	11	2	75	60	1.989	0.010	0.503	0.067	0.002	2.985
15	10	11	2	90	90	2.063	0.018	0.873	0.075	0.002	2.667
16	10	5	4	90	35	2.104	0.016	0.760	0.074	0.002	2.703
17	10	11	4	90	35	2.141	0.014	0.654	0.081	0.003	3.704
18	6	7	2	60	60	1.942	0.018	0.927	0.057	0.001	1.754
19	6	5	2	90	35	2.041	0.016	0.784	0.068	0.002	2.941
20	8	7	2	75	60	1.934	0.018	0.931	0.056	0.001	1.786
21	10	7	0	60	35	2.013	0.014	0.695	0.064	0.002	3.125
22	10	5	0	90	60	2.036	0.014	0.688	0.069	0.002	2.899
23	10	5	4	60	60	2.023	0.012	0.593	0.066	0.002	3.030
24	10	11	0	90	60	2.072	0.006	0.290	0.076	0.003	3.947
25	8	7	2	75	60	1.936	0.020	1.033	0.057	0.002	3.509
26	6	5	2	60	90	1.941	0.018	0.927	0.059	0.002	3.390
27	8	5	0	90	90	1.951	0.008	0.410	0.060	0.002	3.333
28	6	7	0	75	90	1.927	0.018	0.934	0.056	0.001	1.786
29	8	11	4	60	90	1.976	0.018	0.911	0.065	0.001	1.538
30	8	5	0	60	90	1.909	0.012	0.629	0.056	0.001	1.786
31	10	7	2	75	35	2.037	0.016	0.785	0.066	0.002	3.030
32	8	7	2	75	60	1.934	0.014	0.724	0.055	0.001	1.818
33	8	7	2	75	60	1.936	0.004	0.207	0.057	0.001	1.754
34	6	11	0	90	90	2.010	0.008	0.398	0.070	0.002	2.857
35	8	7	4	90	60	1.982	0.006	0.303	0.060	0.001	1.667
36	6	11	0	60	60	1.987	0.016	0.805	0.067	0.002	2.985
37	8	11	0	60	35	2.003	0.008	0.399	0.068	0.002	2.941
38	6	5	0	75	60	1.964	0.016	0.815	0.061	0.001	1.639
39	6	5	4	90	60	2.023	0.014	0.692	0.066	0.002	3.030
40	8	5	4	60	35	1.996	0.014	0.701	0.062	0.002	3.226
41	8	11	0	90	35	2.046	0.012	0.587	0.072	0.002	2.778
42	6	5	0	60	35	1.988	0.020	1.006	0.063	0.002	3.175
43	6	5	4	75	90	1.975	0.012	0.608	0.061	0.002	3.279
44	8	5	2	75	35	1.991	0.012	0.603	0.063	0.002	3.175
45	8	7	2	75	60	1.936	0.014	0.723	0.057	0.001	1.754
46	8	7	2	90	90	1.943	0.006	0.309	0.057	0.001	1.754
47	6	11	2	60	90	1.977	0.018	0.910	0.066	0.002	3.030
48	6	7	0	90	35	2.012	0.016	0.795	0.063	0.002	3.175

Table 3 Effect summary

Source	Log Worth	*P* Value
ε	64.687	0.000
$\gamma \times \gamma$	60.285	0.000
κ	58.844	0.000
γ	55.052	0.000
$\alpha \times \alpha$	54.126	0.000
λ	50.353	0.000
α	48.254	0.000
$\varepsilon \times \varepsilon$	40.055	0.000
$\kappa \times \kappa$	30.854	0.000
$\lambda \times \lambda$	26.278	0.000

Tab. 4 and Tab. 5 show the sorted parameter estimates for all statistically significant effects on R_a and Δd, sorted by the *t*-ratio values that reflect the strength of their effect on the output parameters. Higher estimate values indicate a stronger effect, while negative and positive estimate values indicate the direction of this effect. Negative values for the effects and the square of the effects indicate that an increase in these factors leads to a decrease in R_a and Δd, while positive values for effects indicate that their increase leads to an increase in R_a and Δd. The statistical significance of the effects is confirmed by very low values of Prob > |*t*| and high *t*-ratio values.

Fig. 2 shows a visual assessment of the goodness of fit of the model by analysing the actual by predicted plots for both output parameters. The plots show the relationship between the experimental values and the model predictions. The arrangement of the points close to the diagonal line in both plots indicates the high accuracy of the model and confirms its ability to reliably predict the values of the output parameters based on the predefined input parameters.

Tab. 6 shows the model quality data for each output parameter based on the summary of the fit. High values of the coefficient of determination (R^2) and the adjusted coefficient of determination (R^2_{adj}), which are close to 1, indicate a high degree of agreement of the model with the experimental data. More than 99% of the variability in R_a and Δd can be explained by the factors included in the model. The root mean square error (RMSE) values for R_a

(0.000535) and Δd (0.000324) are very low compared to the mean of the response (MR) values, indicating minimal error between the predicted and actual values, thus confirming the quality of the model.

Table 4 Sorted parameter estimates (R_a)

Term	Estimate	Std Error	*t*-ratio	Prob > |*t*|
ε	−0.028702	9.474×10^{-5}	−302.9	< .0001*
$\gamma \times \gamma$	0.0973144	0.000397	245.12	< .0001*
κ	0.0212687	0.000095	224.08	< .0001*
γ	−0.097348	0.00055	−176.9	< .0001*
$\alpha \times \alpha$	0.0151903	0.000091	167.02	< .0001*
λ	0.0217975	0.000165	132.02	< .0001*
α	−0.033349	0.000288	−115.8	< .0001*
$\varepsilon \times \varepsilon$	0.0119896	0.000173	69.36	< .0001*
$\kappa \times \kappa$	0.0068083	0.000175	38.81	< .0001*
$\lambda \times \lambda$	0.0076157	0.000263	28.92	< .0001*

Table 5 Sorted parameter estimates (Δd)

Term	Estimate	Std Error	*t*-ratio	Prob > |*t*|
$\alpha \times \alpha$	0.0030682	5.517×10^{-5}	55.62	< .0001*
$\gamma \times \gamma$	0.0103025	0.000241	42.78	< .0001*
ε	−0.002423	5.747×10^{-5}	−42.17	< .0001*
α	−0.006743	0.000175	−38.61	< .0001*
κ	0.0021171	5.757×10^{-5}	36.77	< .0001*
γ	−0.010167	0.000334	−30.47	0.4432
λ	0.001146	0.0001	11.44	< .0001*
$\varepsilon \times \varepsilon$	0.0008443	0.000105	8.05	< .0001*
$\kappa \times \kappa$	0.0005764	0.000106	5.42	< .0001*
$\lambda \times \lambda$	0.0001238	0.00016	0.78	< .0001*

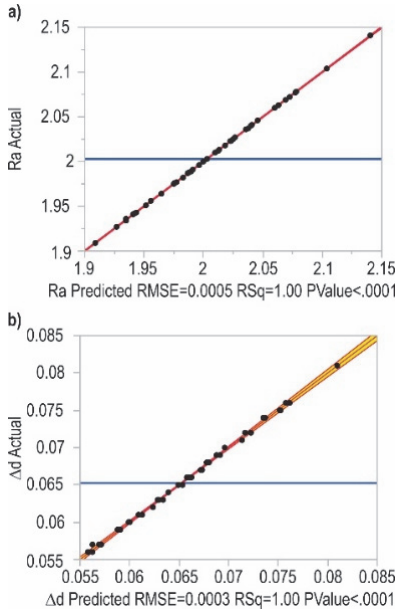

Figure 2 Actual by predicted plot, a) R_a, b) Δd

Table 6 Summary of fit

Parameter	Value	
	R_a	Δd
R^2	0.999916	0.998083
R^2_{adj}	0.999893	0.997565
RMSE	0.000535	0.000324
MR	2.002854	0.06525

The analysis of variance (ANOVA) of the regression models for R_a and Δd presented in Tab. 7 and Tab. 8 shows that the developed models are statistically significant and reliable. The F Ratio values are exceptionally high, indicating that the input parameters have a strong influence on the variations in R_a and Δd. Low values of Prob > F (less than 0.0001) confirm the statistical significance of the models, which means that the probability that these results are random is extremely low. High F Ratio values indicate that the models effectively explain the variations in the data, while the small values of the sum of squared errors indicate that the models are very accurate in predicting the output parameters.

Table 7 Analysis of variance (R_a)

Source	DF	Sum of Squares	Mean Square	F Ratio	Prob > F
Model	10	0.12608940	0.012609	44083.88	< .0001*
Error	37	0.00001058	2.86×10^{-7}	/	/
C. Total	47	0.12609998	/	/	/

Table 8 Analysis of variance (Δd)

Source	DF	Sum of Squares	Mean Square	F Ratio	Prob > F
Model	10	0.00202711	0.000203	1926.341	< .0001*
Error	37	0.00000389	1.052×10^{-7}	/	/
C. Total	47	0.00203100	/	/	/

The adequacy of the model was verified through the analysis of studentized residuals plot, residual by row plot, and residual normal quantile plot. Fig. 3 shows the studentized residuals for R_a and Δd. For both output parameters, the residuals are randomly distributed around the zero line and do not fall outside the interval (95% prediction interval, Bonferroni correction), indicating a good fit of the model and the absence of outliers.

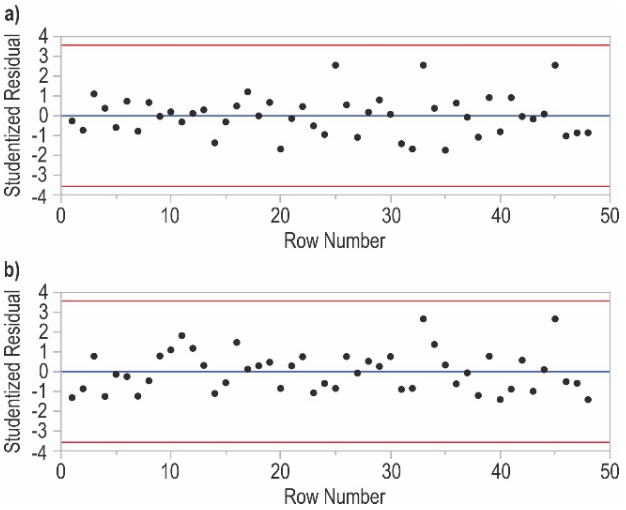

Figure 3 Externally studentized residuals with 95% simultaneous limits, a) R_a, b) Δd

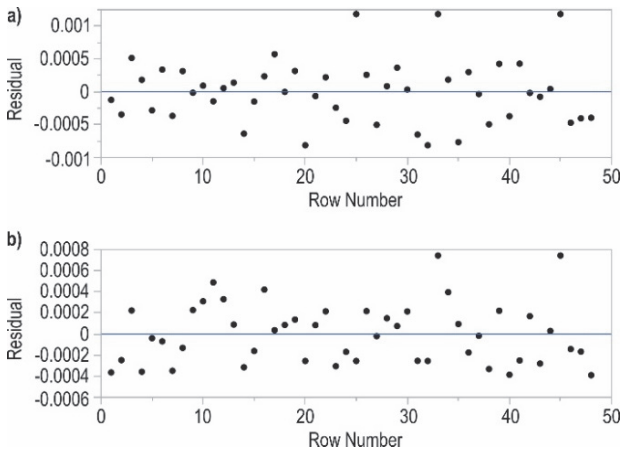

Figure 4 Residual by row plot, a) R_a, b) Δd

Fig. 4 shows the distribution of the residuals by rows of experimental points. The residuals are randomly distributed around the zero line and show no trend, indicating that there are no structural errors and confirming the unbiasedness of the model.

The assessment of the normality of the residuals distribution in the models is shown through the residual normal quantile plots presented in Fig. 5 for both output parameters. Since the points in both cases follow the diagonal line, which represents the ideal normal distribution of the residuals, and do not fall outside the range, this indicates that the residuals are normally distributed and show no significant deviations from normality.

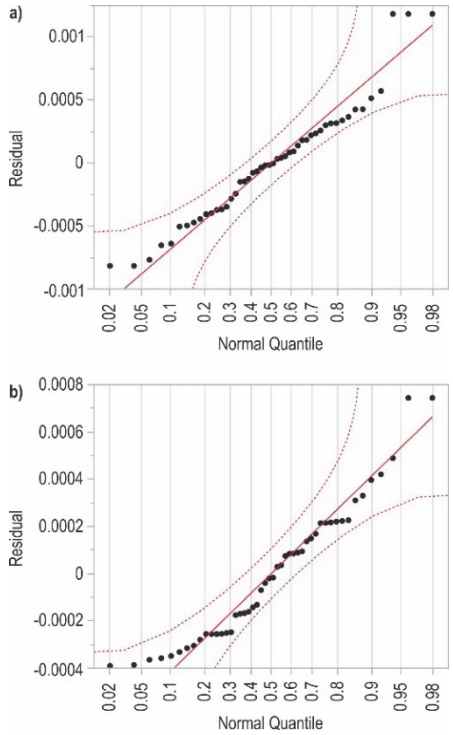

Figure 5 Residual normal quantile plot, a) R_a, b) Δd

Through the analysis, the following regression equations were obtained, which represent mathematical models for predicting the output parameters based on the defined input parameters.

$$R_a = 2.91507888 - 0.05465032 \cdot \alpha - 0.16220180 \cdot \gamma - \\ -0.00302546 \cdot \varepsilon - 0.00312096 \cdot \kappa + 0.00262648 \cdot \lambda + \\ +0.00379756 \cdot \alpha^2 + 0.01081271 \cdot \gamma^2 + 0.00001585 \cdot \\ \cdot \varepsilon^2 + 0.00003026 \cdot \kappa^2 + 0.00121850 \cdot \lambda^2 \quad (2)$$

$$\Delta d = 0.17237513 - 0.01104210 \cdot \alpha - 0.01712556 \cdot \gamma - \\ -0.00022766 \cdot \varepsilon - 0.00024313 \cdot \kappa + 0.00035936 \cdot \lambda + \\ +0.00076705 \cdot \alpha^2 + 0.00114472 \cdot \gamma^2 + 0.00000112 \cdot \\ \cdot \varepsilon^2 + 0.00000256 \cdot \kappa^2 + 0.00001981 \cdot \lambda^2 \quad (3)$$

3.2 Correlation Analysis of Output Parameters

To better understand the process, the potential relationship between changes in surface roughness and dimensional deviations was determined. This potential relationship was identified through bivariate analysis and regression analysis, which allows quantification of the degree and direction of correlation between the output parameters.

Fig. 6 shows the bivariate fit diagram illustrating the relationship between Δd and R_a. The experimental data points are shown as dots in the diagram, while the regression line shows the degree of their association. The clustering of the points near the regression line indicates a high correlation between the parameters, which means that variations in R_a have a direct influence on the Δd. Within the graph, the Pearson correlation coefficient (R) is displayed, which measures the strength and direction of the relationship between the parameters. The value $R = 0.9451$ indicates a very strong positive correlation, which means that an increase in R_a leads to an increase in Δd. The bivariate normal ellipse $P = 0.95$ represents the 95% data density interval, which means that 95% of the data points lie within this interval. A narrow ellipsoid confirms a strong correlation.

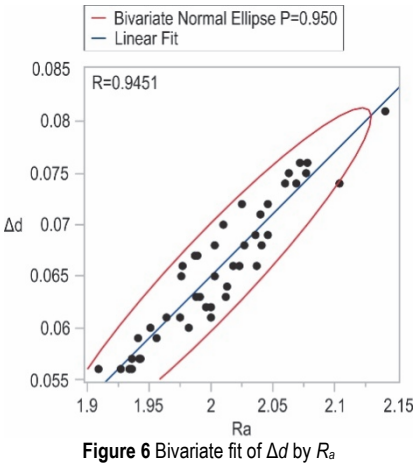

Figure 6 Bivariate fit of Δd by R_a

The statistical indicators for the quality of the model are shown in Tab. 9 and Tab. 10 by the summary of fit and ANOVA. The R^2 value of 0.893206 for the linear fit shows that 89.3% of the variation in Δd can be explained by changes in R_a, indicating a very strong correlation. The values of the RMSE and the MR indicate a high degree of model accuracy. The ANOVA confirms the statistical significance of the model in view of the high F Ratio values and the fact that the Prob > F values are less than 0.05.

Table 9 Summary of fit

Parameter	Value
R^2	0.893206
R^2_{adj}	0.890884
RMSE	0.002174
MR	0.06525

Table 10 Analysis of variance

Source	DF	Sum of Squares	Mean Square	F Ratio	Prob > F
Model	1	0.00181410	0.001814	384.7345	< .0001*
Error	46	0.00021690	4.715×10^{-5}		
C. Total	47	0.00203100			

Based on the analysis, the following linear function was obtained to describe the relationship between R_a and Δd:

$$\Delta d = -0.1749977 + 0.1199425 \cdot R_a \quad (4)$$

4 CONFIRMATION

The validation of the regression equations obtained was carried out through nine additional experiments using combinations of input parameters that were not included in the initial modelling. The effectiveness of the modelling was assessed by calculating the percentage errors, as detailed in Tab. 11. Fig. 7 illustrates the minimum, mean, and maximum values of these percentage errors.

Table 11 Confirmation experiments results

No.	γ / °	α / °	λ / °	κ / °	ε / °	Measured		Prediction		Percentage error		
						R_a / µm	Δd / mm	R_a / µm	Δd / mm	PE_{R_a} / %	$PE_{\Delta d}$ / %	$PE_{\Delta d=f(R_a)}$ / %
1.	10	11	4	90	90	2.083	0.076	2.0830	0.07611	0.000	0.145	1.500
2.	8	7	0	60	90	1.892	0.053	1.8914	0.05211	0.032	1.679	1.981
3.	6	7	4	60	60	1.962	0.058	1.9618	0.05787	0.010	0.224	4.052
4.	10	7	2	90	35	2.066	0.070	2.0658	0.06894	0.010	1.514	4.029
5.	8	5	2	75	60	1.953	0.060	1.9529	0.05993	0.005	0.117	1.217
6.	6	11	0	75	90	1.982	0.064	1.9817	0.06590	0.015	2.969	1.953
7.	10	5	0	75	60	2.008	0.066	2.0077	0.06609	0.015	0.136	0.197
8.	8	11	2	90	35	2.056	0.073	2.0556	0.07304	0.019	0.055	1.890
9	6	5	4	60	35	2.018	0.065	2.0180	0.06458	0.000	0.646	3.185

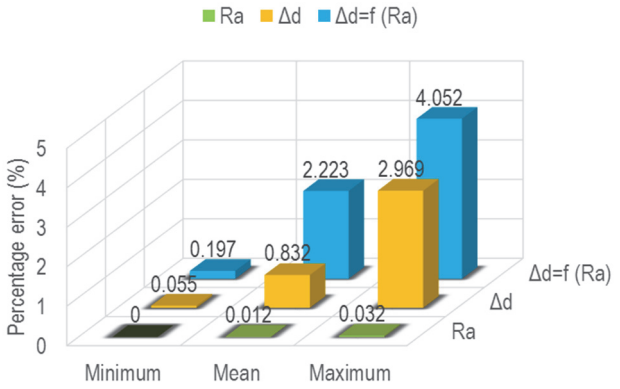

Figure 7 Confirmation experiments percentage errors

5 DISCUSSION

The effects of a change in the output parameters as a function of the input parameters are displayed visually in the prediction profiler (Fig. 8). In addition to the trends in the changes in the output parameters, the prediction profiler also shows the minimum predicted value of the output parameters and the confidence interval for the mean response. For both R_a and Δd, optimal values were determined for the following cutting insert angles γ = 8°, α = 7°, λ = 0°, κ = 60° and ε = 90°, namely R_a = 1.890808 [1.89024, 1.89137] (µm) and Δd = 0.052111 [0.05177, 0.05245] (mm).

The results show that a lower Δd and a better R_a are achieved with medium values of the rake and clearance angle, smaller values of the inclination angle and approach angle and with larger values of the nose angle.

The influence of the γ and clearance angle has a similar tendency on the Δd and R_a. As the γ and α increase, the Δd and R_a initially improve and then deteriorate. As α increases, the friction between the flank surface and the workpiece decreases. In addition, the sharpness of the cutting edge increases with increasing γ and α, and the cutting edge penetrates the workpiece more easily. This leads to a reduction in cutting forces, a lower cutting temperature and less cutting insert wear. As a result, Δd and R_a are reduced. However, with a further increase in the γ and α, the strength of the cutting edge decreases, the heat is more difficult to dissipate, the wear on the rake and clearance surface increases and the tool life decreases. Therefore, the Δd and R_a increase with a further increase in the γ and α.

As the κ decreases, the radial component of the cutting force increases, which can lead to vibrations. However, the radial component of the cutting force has not yet reached a critical value above which the vibrations increase, which can lead to a deterioration in the Δd and R_a. At the same time, the strength of the cutting insert increases with a reduction in the κ, as the heat can be dissipated more easily from the cutting zone. If the κ is reduced, the width of the cutting edge is greater so that the heat is distributed over a larger area, which leads to an increase in tool life. A reduction in the κ therefore results in a smaller Δd and a lower R_a.

As the λ decreases, the turning insert tip is at a lower point relative to the cutting edge. When the cutting edge enters in the workpiece, the contact point is on the cutting edge and protects the turning insert tip from dynamic loads. Smaller values of the λ increase the strength of the turning insert tip and resistance to dynamic loads. In connection with the previous one, there is less cutting insert wear and the result is less Δd and less R_a.

Increasing the ε increases the cutting edge strength, i.e. a stronger turning insert is obtained. A stronger turning insert wears less. The result is less Δd and less R_a.

The results obtained indicate the influence of tool wear on the results achieved. This is confirmed by the measurement results of the flank wear. The flank wear of the cutting insert for the case where the smallest R_a and the smallest Δd are achieved is VB = 0.249 mm, while for the case of the highest R_a and the largest Δd it is VB = 0.361 mm.

The results of the confirmation tests show small deviations of the prediction from the measured results. The percentage prediction errors of PE_{R_a} = 0.000-0.032 %, $PE_{\Delta d}$ = 0.055-2.969 % and $PE_{\Delta d=f(R_a)}$ = 0.197-4.052 % indicate that the dry turning process of Ti6Al4V alloy is correctly modelled and practically applicable.

Finally, the calculated standard deviations and coefficients of variation demonstrate that the obtained results have low uncertainty.

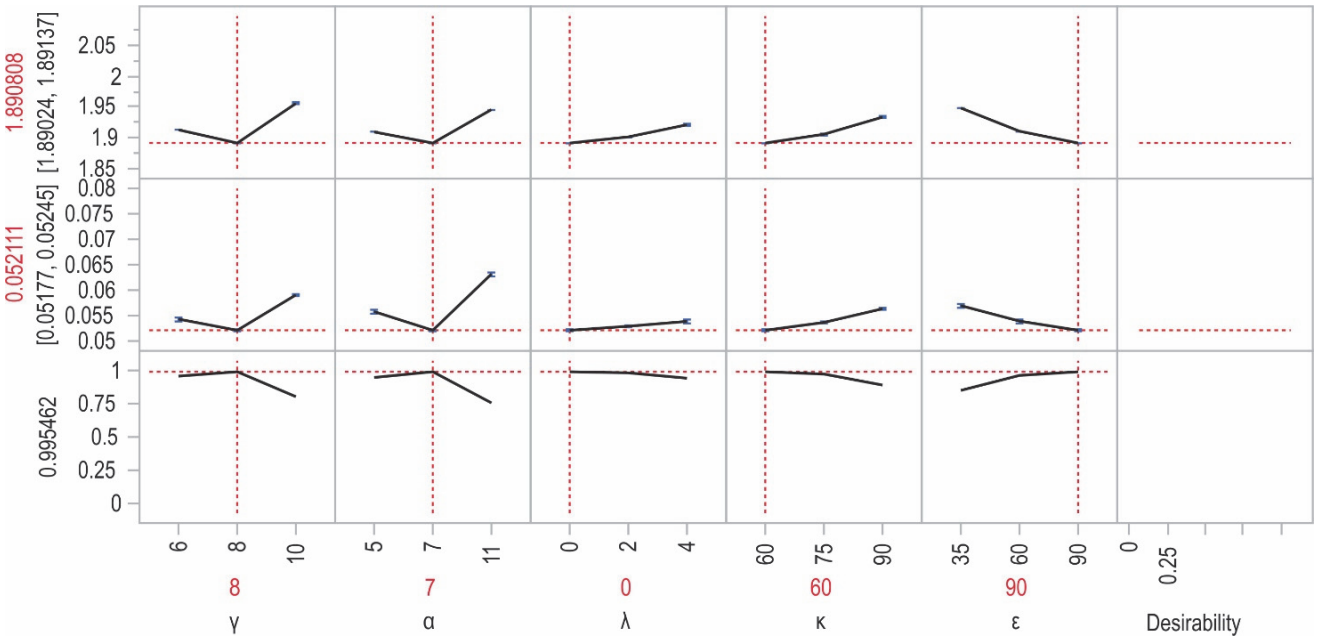

Figure 8 Prediction profiler

6 CONCLUSION

In the study, the modelling of cutting insert angles was analysed in terms of R_a and Δd.

Different combinations of cutting insert angles resulted in varying values for R_a and Δd. The Δd values ranged from 0.053 mm to 0.081 mm, showing a percentage difference of 52.83%. The R_a values ranged from 1.892 mm to 2.141 mm, with a percentage difference of 13.16%. This indicates that altering the cutting insert angles can enhance both the accuracy of turning and the quality of the machined surface. Furthermore, the influence of the cutting insert angle on dimensional accuracy was found to be more significant, while its impact on surface roughness was less pronounced.

The results demonstrate that dry turning of Ti6Al4V alloys can be performed effectively with the following insert angles: $\gamma = 8°$, $\alpha = 7°$, $\lambda = 0°$, $\kappa = 60°$ and $\varepsilon = 90°$. These specific angles yield the lowest Δd and the smallest R_a. Additionally, a strong correlation was observed between the output parameters, with cutting insert wear being the dominant influencing factor.

Confirmation tests were conducted to verify the accuracy of the test results. The maximum percentage modelling errors were 2.969% for Δd, 0.032% for R_a, and 4.052% for Δd as a function of R_a. These errors suggest that the regression equations developed could be practically applied in a real manufacturing environment.

7 REFERENCES

[1] Che-Haron, C. H. & Jawaid, A. (2005). The effect of machining on surface integrity of titanium alloy Ti-6% Al-4% V. *Journal of Materials Processing Technology*, *166*(2), 188-192. https://doi.org/10.1016/j.jmatprotec.2004.08.012

[2] Ramesh, S., Karunamoorthy, L., & Palanikumar, K. (2008). Surface Roughness Analysis in Machining of Titanium Alloy. *Materials and Manufacturing Processes*, *23*(2), 174-181. https://doi.org/10.1080/10426910701774700

[3] Jianxin, D., Yousheng, L., & Wenlong, S. (2008). Diffusion wear in dry cutting of Ti-6Al-4V with WC/Co carbide tools. *Wear*, *265*(11-12), 1776-1783. https://doi.org/10.1016/j.wear.2008.04.024

[4] Tsourveloudis, N. C. (2010). Predictive Modeling of the Ti6Al4V Alloy Surface Roughness. *Journal of Intelligent & Robotic Systems*, *60*(3-4), 513-530. https://doi.org/10.1007/s10846-010-9427-6

[5] Fan, Y. H., Zheng, M. L., Zhang, D. Q., Yang, S. C., & Cheng, M. M. (2011). Static and Dynamic Characteristic of Cutting Force when High-Efficiency Cutting Ti-6Al-4V. *Advanced Materials Research*, *305*, 122-128. https://doi.org/10.4028/www.scientific.net/AMR.305.122

[6] Wang, X. Q., Ai, X., Zhao, J., Fu, X. L., & Pan, Y. Z. (2012). Tool Life Prediction and Cutting Parameter Optimization for Coated Carbide in Ti6Al4V Turning. *Advanced Materials Research*, *426*, 186-189. https://doi.org/10.4028/www.scientific.net/AMR.426.186

[7] Kosaraju, S. & Anne, V. G. (2013). Optimal machining conditions for turning Ti-6Al-4V using response surface methodology. *Advances in Manufacturing*, *1*(4), 329-339. https://doi.org/10.1007/s40436-013-0047-9

[8] Xie, J., Luo, M. J., Wu, K. K., Yang, L. F., & Li, D. H. (2013). Experimental study on cutting temperature and cutting force in dry turning of titanium alloy using a non-coated micro-grooved tool. *International Journal of Machine Tools and Manufacture*, *73*, 25-36. https://doi.org/10.1016/j.ijmachtools.2013.05.006

[9] Sun, S., Brandt, M., & Mo, J. P. (2014). Evolution of tool wear and its effect on cutting forces during dry machining of Ti-6Al-4V alloy. *Proceedings of the Institution of Mechanical Engineers, Part B: Journal of Engineering Manufacture*, *228*(2), 191-202. https://doi.org/10.1177/0954405413500243

[10] Sun, F. J., Qu, S. G., Pan, Y. X., Li, X. Q., & Li, F. L. (2015). Effects of cutting parameters on dry machining Ti-6Al-4V alloy with ultra-hard tools. *International Journal of Advanced Manufacturing Technology*, *79*(1-4), 351-360. https://doi.org/10.1007/s00170-014-6717-3

[11] Chetan, Behera, B. C., Ghosh, S., & Rao, P. V. (2016). Wear behavior of PVDTiN coated carbide inserts during machining of Nimonic 90 and Ti6Al4V superalloys under dry and MQL conditions. *Ceramics International*, *42*(13), 14873-14885. https://doi.org/10.1016/j.ceramint.2016.06.124

[12] Sargade, V. G., Nipanikar, S. R., & Meshram, S. M. (2016). Analysis of surface roughness and cutting force during turning of Ti6Al4V ELI in dry environment. *International Journal of Industrial Engineering Computations*, *7*(2), 257-266. https://doi.org/10.5267/j.ijiec.2015.10.004

[13] Umbrello, D., Bordin, A., Imbrogno, S., & Bruschi, S. (2017). 3D finite element modelling of surface modification in dry and cryogenic machining of EBM Ti6Al4V alloy. *CIRP Journal of Manufacturing Science and Technology*, *18*, 92-100. https://doi.org/10.1016/j.cirpj.2016.10.004

[14] Celik, Y. H., Kilickap, E., & Guney, M. (2017). Investigation of cutting parameters affecting on tool wear and surface roughness in dry turning of Ti-6Al-4V using CVD and PVD coated tools. *Journal of the Brazilian Society of Mechanical Sciences and Engineering*, *39*(6), 2085-2093. https://doi.org/10.1007/s40430-016-0607-6

[15] Sanchez Hernandez, Y., Trujillo Vilches, F. J., Bermudo Gamboa, C., & Sevilla Hurtado, L. (2018). Experimental Parametric Relationships for Chip Geometry in Dry Machining of the Ti6Al4V Alloy. *Materials*, *11*(7), 1260. https://doi.org/10.3390/ma11071260

[16] Caggiano, A. (2018). Tool Wear Prediction in Ti-6Al-4V Machining through Multiple Sensor Monitoring and PCA Features Pattern Recognition. *Sensors*, *18*(3), 823. https://doi.org/10.3390/s18030823

[17] Dargusch, M. S., Sun, S., Kim, J. W., Li, T., Trimby, P., & Cairney, J. (2018). Effect of tool wear evolution on chip formation during dry machining of Ti-6Al-4V alloy. *International Journal of Machine Tools and Manufacture*, *126*, 13-17. https://doi.org/10.1016/j.ijmachtools.2017.12.003

[18] Sanchez Hernandez, Y., Trujillo Vilches, F. J., Bermudo Gamboa, C., & Sevilla Hurtado, L. (2019). Online Tool Wear Monitoring by the Analysis of Cutting Forces in Transient State for Dry Machining of Ti6Al4V Alloy. *Metals*, *9*(9), 1014. https://doi.org/10.3390/met9091014

[19] You, S. H., Lee, J. H., & Oh, S. H. (2019). A Study on Cutting Characteristics in Turning Operations of Titanium Alloy used in Automobile. *International Journal of Precision Engineering and Manufacturing*, *20*(2), 209-216. https://doi.org/10.1007/s12541-019-00027-x

[20] Liang, X., Liu, Z., Yao, G., Wang, B., & Ren, X. (2019). Investigation of surface topography and its deterioration resulting from tool wear evolution when dry turning of titanium alloy Ti-6Al-4V. *Tribology International*, *135*, 130-142. https://doi.org/10.1016/j.triboint.2019.02.049

[21] Wang L., Yuan M., Li Y., Huang K., Tian Y., Zhang Q., & Wang J. (2020). Cutting Mechanism of WC-8Co Cemented Carbide for Dry Turning of Ti6Al4V Before and After Pulsed Electromagnetic Coupling Processing. *Rare Metal Materials and Engineering*, *49*(12), 4016-4022

[22] Kumar, P. & Misra, J. P. (2020). Process modeling and optimization using ANN and RSM during dry turning of titanium alloy used in automotive industry. *Proceedings of the Institution of Mechanical Engineers, Part D: Journal of Automobile Engineering*, *235*(7), 2040-2050. https://doi.org/10.1177/0954407020969255

[23] De Maddis, M., Lunetto, V., Razza, V., & Russo Spena, P. (2022). Infrared Thermography for Investigation of Surface Quality in Dry Finish Turning of Ti6Al4V. *Metals*, *12*(1), 154. https://doi.org/10.3390/met12010154

[24] Guvenc, M. A., Bilgic, H. H., & Mistikoglu, S. (2023). Identification of chatter vibrations and active vibration control by using the sliding mode controller on dry turning of titanium alloy (TI6AL4V). *Facta Universitatis, Series: Mechanical Engineering*, *21*(2), 307-322. https://doi.org/10.22190/FUME210728067G

[25] Martin-Bejar, S., Trujillo Vilches, F. J., Herrera Fernandez, M., Bermudo Gamboa, C., & Sevilla Hurtado, L. (2024). Cutting parameters influence on surface integrity of dry-turned Ti6Al4V alloy. *Proceedings of the Institution ofMechanical Engineers, Part L: Journal of Materials: Design and Applications*, *238*(2), 245-262. https://doi.org/10.1177/14644207231195749

[26] Cozzolino, E., Franchitti, S., Borrelli, R., & Astarita, A. (2024). Sustainability assessment of electron beam melted Ti6Al4V machining: energy consumption and lubricant use. *Materials and Manufacturing Processes*, *39*(9), 1247-1259. https://doi.org/10.1080/10426914.2024.2311395

[27] Vukelic, D., Simunovic, K., Kanovic, Z., Saric, T., Doroslovacki, K., Prica, M., & Simunovic, G. (2022). Modelling surface roughness in finish turning as a function of cutting tool geometry using the response surface method, Gaussian process regression and decision tree regression. *Advances in Production Engineering & Management*, *17*(3), 367-380. https://doi.org/10.14743/apem2022.3.442

[28] Vukelic, D., Milosevic, A., Ivanov, V., Kocovic, V., Santosi, Z., Sokac, M., & Simunovic, G. (2024). Modelling of Flank and Crater Wear during Dry Turning of AISI 316L Stainless Steel as a Function of Tool Geometry Using the Response Surface Design. *TehnickiVjesnik - Technical Gazette*, *31*(4), 1376-1384. https://doi.org/10.17559/TV-20231226001235

[29 Vukelic, D., Prica, M., Ivanov, V., Jovicic, G., Budak, I., & Luzanin, O. (2022). Optimization of Surface Roughness Based on Turning Parameters and Insert Geometry. *International Journal of Simulation Modelling*, *21*(3), 417-428. https://doi.org/10.2507/IJSIMM21-3-607

[30] Saric, T., Vukelic, D., Simunovic, K., Svalina, I., Tadic, B., Prica, M., & Simunovic, G. (2020). Modelling and Prediction of Surface Roughness in CNC Turning Process using Neural Networks. *TehnickiVjesnik - Technical Gazette*, *27*(6), 1923-1930. https://doi.org/10.17559/TV-20200818114207

[31] Dragicevic, M., Begovic, E., Ekinovic, S., & Peko, I. (2023). Multi-Response Optimization in MQLC Machining Process of Steel St50-2 Using Grey-Fuzzy Technique. *TehnickiVjesnik - Technical Gazette*, *30*(1), 248-255. https://doi.org/10.17559/TV-20220222080715

[32] Van, A. L., Nguyen, T. T., & Dang, X. B. (2023). Optimization of Rough Self-Propelled Rotary Turning Parameters in terms of Total Energy Consumption and Surface Roughness. *TehnickiVjesnik - Technical Gazette*, *30*(6), 1728-1736. https://doi.org/10.17559/TV-20230202000308

[33] Milosevic, A., Simunovic, G., Kanovic, Z., Simunovic, K., Santosi, Z., Sokac, M., &Vukelic, D. (2024). Comprehensive evaluation of dimensional deviation, flank wear, surface roughness and material removal rate in dry turning of C45 steel. *Facta Universitatis, Series: Mechanical Engineering*, *22*(4), 547-566. https://doi.org/10.22190/FUME240403024M

[34] Vukelic, D., Milosevic, A., Ivanov, V., Kocovic, V., Santosi, Z., Sokac, M., & Simunovic, G. (2024). Modelling and optimization of dimensional accuracy and surface roughness in dry turning of Inconel 625 alloy. *Advances in Production Engineering & Management*, *19*(3), 371-385. https://doi.org/10.14743/apem2024.3.513

[35] Milosevic, A., Simunovic, G., Kanovic, Z., Simunovic, K., Mitrovic, S., Buchmeister, B., & Vukelic, D. (2026). Modelling and Optimization of Grinding and Wheel Parameters in Cylindrical Longitudinal Machining of Tool Steel, *Facta Universitatis, Series: Mechanical Engineering*, https://doi.org/10.22190/FUME260110002M

Contact information:

Djordje VUKELIC, PhD
(Corresponding author)
University of Novi Sad,
Faculty of Technical Sciences,
Trg Dositeja Obradovica 6, 21000 Novi Sad, Serbia
E-mail: vukelic@uns.ac.rs

Aleksandar MILOSEVIC, MSc
University of Novi Sad,
Faculty of Technical Sciences,
Trg Dositeja Obradovica 6, 21000 Novi Sad, Serbia

Goran SIMUNOVIC, PhD
University of Slavonski Brod,
Mechanical Engineering Faculty,
Trg Ivane Brlic Mazuranic 2, 35000 Slavonski Brod, Croatia

Vitalii IVANOV, PhD
Sumy State University,
Faculty of Technical Systems and Energy Efficient Technologies,
Rymskogo-Korsakova 2, 40007 Sumy, Ukraine

Zeljko SANTOSI, PhD
University of Novi Sad,
Faculty of Technical Sciences,
Trg Dositeja Obradovica 6, 21000 Novi Sad, Serbia

Mario SOKAC, PhD
University of Novi Sad,
Faculty of Technical Sciences,
Trg Dositeja Obradovica 6, 21000 Novi Sad, Serbia

Slobodan MITROVIC, PhD
University of Kragujevac,
Faculty of Engineering,
Sestre Janjic 6, 34000 Kragujevac, Serbia